IN-FLIGHT ALIGNMENT IN INS-AIDING WITH SWITCHED FEEDFORWARD/FEEDBACK OF ERROR ESTIMATES

Jacques Waldmann, jacques@ita.br
Instituto Tecnológico de Aeronáutica – CTA-ITA-IEES – 12228-900 São José dos Campos – SP - Brazil

Abstract. *Unmanned air vehicles often resort to a low-cost inertial measurement unit (IMU) in an inertial navigation system (INS) to estimate position and velocity. Stand-alone INS operation yields unbounded estimation errors that depend on IMU's initial alignment errors, measurement noise, accelerometer bias, and rate-gyro drift. Such behavior motivates INS aiding by auxiliary position and velocity sensors to limit navigation error. Acceleration maneuvers and IMU rotation with respect to the vehicle are used to enhance the observability of INS error dynamics, in conjunction with Kalman filter-based sensor fusion to estimate position and velocity errors, IMU misalignment and sensor errors. This work investigates feedforward and feedback of error estimates for INS aiding. Feedforward integration is used to estimate IMU misalignment and sensor errors with adequate accuracy, and then switches to feedback integration for in-flight alignment (IFA), that is INS reset and IMU calibration during operation. A Monte Carlo simulation provides evidence supporting the approach and encourages implementation in low-cost unmanned air vehicles.*

Keywords: *inertial navigation, in-flight alignment, sensor fusion,autonomous vehicles, robotics*

1. INTRODUCTION

An inertial navigation system (INS) estimates position and velocity. The INS comprises computational resources and an inertial measurement unit (IMU) containing accelerometers and rate-gyros capable of measuring specific force and angular rate components. Gimbaled INS implementations (GINS) employ accurate mechanisms to isolate the IMU from the host vehicle's motion and keep alignment with the navigation reference frame. A strapdown configuration (SDINS) employs an IMU rigidly attached to the host vehicle. The IMU sensors provide signals in discrete time and incremental form, and adequate numerical integration provides the desired estimates. The INS can track short-term, abrupt motions, but estimation errors grow unbounded during long operation periods due to the integration of low-frequency errors such as accelerometer bias and rate-gyro drift, which are here assumed to be unknown, constant null offsets. Before entering navigation mode, IMU calibration and alignment – often relative to the North-East-Down frame – make use of leveling and gyrocompassing, which are based on reaction to gravity and earth rate sensing while the vehicle remains stationary at a known location on the ground. More recently, autonomous vehicles resort to a low-cost SDINS aided by additional sensors, and Kalman filter-based sensor fusion is employed to estimate navigation, IMU misalignment and sensor errors (Adam et al., 1999; Roumeliotis et al., 2002; Eck and Geering, 2000; Hafskjold et al., 2000, and Wagner et al., 2003).

Bar-Itzhack and Berman (1988) showed the lack of full observability when estimating IMU misalignment and sensor errors of a stationary GINS with velocity error measurements. Their analysis employed linear navigation and misalignment error dynamics augmented with random constant accelerometer bias and rate-gyro drift. Goshen-Meskin and Bar-Itzhack (1990) departed from the augmented computer-frame velocity error model of a GINS, investigated its observability, and indicated that the ability to maneuver is "a blessing in disguise". That is, though IFA may seem to be less accurate and more complicated than alignment at rest, maneuvers during the IFA phase can excite latent error dynamics. Acceleration maneuvers in a GINS were modeled by a concatenation of piece-wise constant (PWC) specific force segments to circumvent the trajectory-dependent, numerical computation of the observability Grammian of a linear time-varying model. Observability analysis of the PWC linear error dynamics was based on determining the rank of the stripped observability matrix (SOM) after each acceleration segment (Goshen-Meskin and Bar-Itzhack, 1990; Lee *et al.*, 1993). SOM analysis disregarded the actual model mismatch arising from linearization errors during operation and its effect on error estimation accuracy.

Rotorcraft and aerial vehicles with vectorized thrust are capable of PWC acceleration segments without significant attitude maneuvers. Goshen-Meskin and Bar-Itzhack (1990) claimed that covariance simulation and real IFA results showed that the exact nature of acceleration maneuvers is not influential, but their mere existence is paramount for accurate GINS misalignment and IMU error estimation. Thus, insights from SOM analysis seem to apply to other GINS-equipped vehicles and maneuvers. On the other hand, SDINS-equipped vehicles without vectorized thrust must conduct attitude maneuvers to generate accelerations. It is intuitive that maneuvers in acceleration *and* IMU attitude should enhance estimation accuracy, but continuously changing IMU attitude violates the assumption of PWC dynamics, which precludes SOM analysis.

This investigation confirms the benefit of both IMU rotation and PWC acceleration segments on estimation accuracy relative to a GINS undergoing the same acceleration maneuvers. The reader should note that optimal maneuver design for IFA is not within the scope of this work. Instead of a strapdown configuration, here the IMU rotates relative to the host vehicle. IMU rotation does not require the accurate mechanism of a gimbaled INS because what matters is to change the direction of the inertial sensors' sensitive axes relative to gravity and earth angular rate.

Hence, the host vehicle need not maneuver away from the desired path for observability enhancement during IFA. The IMU can be locked in a known attitude relative to the vehicle following the IFA phase. The approach has been inspired by Lee et al. (1993), which employed SOM analysis and concatenated PWC segments of IMU attitude for multiposition alignment on the ground. Notice that vehicle attitude is a by-product of the conventional strapdown configuration at all times, whereas during IFA phase the present approach produces IMU attitude. The inertial sensors are assumed to be aligned with the IMU frame S_b.

The second purpose of this investigation is to evaluate two sensor fusion configurations, feedforward and feedback of navigation and IMU sensor error estimates based on aiding position and velocity sensors. Feedforward aiding employs a Kalman filter linearized about the diverging INS estimates, and removes *a posteriori* the estimated position and velocity errors from the INS output. On the other hand, feedback aiding employs in-flight INS reset and IMU calibration, thus resulting in an extended Kalman filter linearized about the corrected INS output. This work initially resorts to feedforward integration to estimate misalignment and IMU errors with sufficient accuracy, and then switches to feedback integration for INS reset and IMU calibration.

Section 2 presents the navigation and attitude equations, and briefly describes the multirate algorithm and the computer-frame velocity error model for use in the Kalman filter. Section 3 discusses both sensor fusion configurations. Section 4 presents the simulation of stationary and IFA phase of both GINS and rotating IMU mechanizations, and shows the results of the Monte Carlo simulation of switching from feedforward to feedback of error estimates, and analyzes the results. Finally, conclusions are found in Section 5.

2. INERTIAL NAVIGATION, ATTITUDE, AND LINEARIZED DYNAMICS FOR SENSOR FUSION

The following coordinate frames have their origins at the center of the earth: S_i is the inertial frame, S_e is the earth-fixed geographic frame and S_s is the navigation reference frame. Angular rates to recognize are the constant inertial earth rate $\omega^{ei} = \Omega$ of S_e relative to S_i, and the inertial rate $\omega^{si} = \omega$ of S_s relative to S_i. The transport rate is $\omega^{se} = \rho = \omega - \Omega$. Position is denote by vector $\boldsymbol{R}$, and a superscript indicates the coordinate frame in which the time derivative of a vector is observed. Neglecting measurement errors, accelerometers provide the specific force:

$$\mathbf{A}_{sp} = \overset{ii}{\mathbf{R}} - \mathbf{g}_m \tag{1}$$

$g_m = g_m(R)$ is the gravitational pull toward the earth center due to mass attraction, and $\overset{ii}{R}$ is the inertial second derivative, i.e., inertial acceleration. Inertial velocity is:

$$\overset{i}{\mathbf{R}} = \overset{e}{\mathbf{R}} + \mathbf{\Omega} \times \mathbf{R} = \mathbf{V}_e + \mathbf{\Omega} \times \mathbf{R} \tag{2}$$

$V_e = \overset{e}{R}$ is the terrestrial velocity observed from the earth-fixed coordinate frame S_e. From Eq. (2), inertial acceleration is:

$$\overset{ii}{\mathbf{R}} = \overset{i}{\mathbf{V}}_e + \mathbf{\Omega} \times \overset{i}{\mathbf{R}} = \overset{i}{\mathbf{V}}_e + \mathbf{\Omega} \times (\mathbf{V}_e + \mathbf{\Omega} \times \mathbf{R}) \tag{3}$$

The rate of terrestrial velocity as observed from the navigation frame S_s is $\overset{s}{V}_e = \overset{se}{R}$. Since $\overset{i}{V}_e = \overset{s}{V}_e + \omega^{si} \times V_e$, Eq. (3) yields:

$$\overset{ii}{\mathbf{R}} = \overset{s}{\mathbf{V}}_e + (\mathbf{\omega} + \mathbf{\Omega}) \times \mathbf{V}_e + \mathbf{\Omega} \times (\mathbf{\Omega} \times \mathbf{R}) \tag{4}$$

Substitution in Eq. (1) and rearranging yields the navigation equation in vector form:

$$\overset{s}{\mathbf{V}}_e = \mathbf{A}_{sp} - (\mathbf{\omega} + \mathbf{\Omega}) \times \mathbf{V}_e + \mathbf{g} \qquad \mathbf{g} = -\mathbf{\Omega} \times (\mathbf{\Omega} \times \mathbf{R}) + \mathbf{g}_m$$

$$\overset{s}{\mathbf{R}} = \mathbf{V}_e - \mathbf{\rho} \times \mathbf{R} \tag{5}$$

$g = g(R)$ is the local plumb-bob gravity vector. Specific force measurements, a gravity model, and knowledge of initial conditions $V_e(0)$ and $R(0)$ are needed to numerically obtain the solution to Eq. (5) − the inertial estimates $V_{e,INS}(t)$ and $R_{INS}(t)$. Equation (5) is often mechanized to reflect the choice of $S_s \equiv S_{NED}$. The U.S. Department of Defense World Geodetic System (DoD WGS-84) approximates the earth's shape by a geocentric reference ellipsoid, which models earth radius R_e, curvature radii R_E and R_N along East and North directions, respectively, and gravity (Siouris, 1993).

Latitude λ, longitude Λ, and altitude h describe the terrestrial position. From Eq. (5), the continuous-time navigation equations are:

$$\dot{\lambda} = \frac{V_N}{R_N + h} \quad ; \qquad \dot{\Lambda} = \frac{V_E}{(R_E + h)\cos(\lambda)} \quad ; \qquad \dot{h} = -V_D$$

$$\dot{V}_N = A_{sp,N} + \frac{V_N V_D}{(R_N + h)} - V_E \{2\Omega\sin(\lambda) + \frac{V_E \tan(\lambda)}{(R_E + h)}\}$$

$$\dot{V}_E = A_{sp,E} + V_N \{2\Omega\sin(\lambda) + \frac{V_E \tan(\lambda)}{(R_E + h)}\} + V_D \{2\Omega\cos(\lambda) + \frac{V_E}{(R_E + h)}\}$$

$$\dot{V}_D = A_{sp,D} - \frac{V_N V_N}{(R_N + h)} - V_E \{2\Omega\cos(\lambda) + \frac{V_E}{(R_E + h)}\} + g(\lambda, h) \tag{6}$$

$g(\lambda, h) = g_0 (1 + 0.0053 \sin^2(\lambda))(1 - 2h/R_e)$ is a sufficiently accurate approximation of gravity. Inaccurate knowledge about gravity is not among the most significant sources of errors in stand-alone, low-cost INS operation where the effect of IMU errors strongly exceed those due to gravity errors (Jekeli, 1997). Use of accelerometer data in Eq. (6) needs attitude determination, i.e. the transformation from S_b to S_{NED} according to $A_{sp,NED} = D^b_{NED,INS} A_{sp,b,m}$. The subscript m indicates a measured value, whereas *INS* means the INS stand-alone solution. One approach is to compute the direction cosine matrix (DCM) from angular rate measurements and the initial alignment $D^b_{NED,INS}(0)$:

$$\dot{D}^b_{NED,INS} = D^b_{NED,INS} \Omega^{bi}_{b,m} - \Omega^{NEDi}_{NED,INS} D^b_{NED,INS} \tag{7}$$

The entries in skew-symmetric (cross product form) matrix $\Omega^{bi}_{b,m}$ are the components of the angular rate sensed by the IMU's rate-gyro triad. Likewise, skew symmetric matrix $\Omega^{NEDi}_{NED,INS}$ relates to the components of $\omega^{NEDi}_{NED,INS}$:

$$\omega^{NEDi}_{NED,INS} = \omega^{ei}_{NED,INS} + \omega^{NEDe}_{NED,INS} = \Omega_{NED,INS} + \rho_{NED,INS} = \begin{bmatrix} \Omega_{N,INS} \\ 0 \\ \Omega_{D,INS} \end{bmatrix} + \begin{bmatrix} \rho_{N,INS} \\ \rho_{E,INS} \\ \rho_{D,INS} \end{bmatrix} = \begin{bmatrix} (\Omega + \dot{\Lambda}_{INS})\cos(\lambda_{INS}) \\ -\dot{\lambda}_{INS} \\ -(\Omega + \dot{\Lambda}_{INS})\sin(\lambda_{INS}) \end{bmatrix} \tag{8}$$

$\dot{\Lambda}_{INS}, \dot{\lambda}_{INS}, \lambda_{INS}$ are from the INS stand-alone solution to Eq. (6). The INS stand-alone solution to Eq. (6) and Eq. (7) is computed by a multirate algorithm to reduce the computational burden. The algorithm processes IMU discrete-time measurements, that is angular and thrust velocity increments occurring between sensor samples (Bar-Itzhack, 1978; Savage, 1998; Waldmann, 2003). Coning errors arise because finite rotations do not commute, sculling errors are due to incorrect thrust velocity computation as coordinate frames rotate between data samples, and scrolling errors arise from velocity and position updates occurring at distinct rates. Though complex, with intricate compensation terms to attenuate such errors, Savage's multirate approach has been utilized due to its enhanced accuracy. Thrust velocity increments from the accelerometers are transformed from S_b to S_{NED} at a high sampling rate, and terrestrial velocity and position are solved at intermediate and slow rates, respectively. The fast acquisition rate of incremental inertial samples and attitude computation has been set to 400Hz. The INS terrestrial velocity and position are computed at the intermediate and slow rates $1/T_{int}$=200Hz and $1/T_{nav}$=100Hz, respectively. The stand-alone inertial solution diverges due to errors in IMU data and erroneous processing by the multirate algorithm, thus causing linearization errors and model mismatch in the Kalman filter used for fusion of the INS solution with aiding sensors.

2.1. The computer frame velocity error model for Kalman filter-based sensor fusion

Figure 1 shows the most relevant NED coordinate frames and misalignment angles for a brief description of this error model. True, computed, and platform frames, S_t, S_c, and S_p, respectively, are located at the actual and estimated positions. S_c is perfectly known, albeit it is incorrect. If initial alignment and inertial data were error free, the integration of Eq. (7) would produce D^b_t. However, accelerometer bias and rate-gyro drift yield $D^b_p = D^b_{NED,INS}$. $\delta\theta$ is a small misalignment angle vector due to errors in the estimated position. $\delta\theta$ rotates S_t into alignment with S_c, and is represented in S_c as:

$$\delta\theta_c = [\Delta R_E/(R_E(\lambda) + h) \quad -\Delta R_N/(R_N(\lambda) + h) \quad -\Delta R_E \tan(\lambda)/(R_E(\lambda) + h)]^T \tag{9}$$

R_E and R_N are the earth's curvature radii, and ΔR_E and ΔR_N are position errors. The small misalignment angle vector ψ is due to rate-gyro drift, and rotates S_c into alignment with S_p. Use of the computer frame S_c for the error model is

attractive because it renders the misalignment rate $\overset{\bullet}{\psi}{}^{c}$ uncoupled from both position and terrestrial velocity errors. The total misalignment angle $\phi = \delta\theta + \psi$ from S_t to S_p can be estimated from Eq. (9) using the INS solution to Eq. (6), and the Kalman filter estimates of ψ and $\varDelta R$.
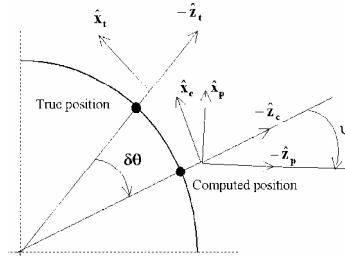

Figure 1 – True, computed, and platform NED coordinate frames and respective misalignment angles

Assuming a spherical earth and the IMU path in the vicinity of the earth's surface, the computer-frame position error model was obtained and further elaborated to show its equivalence to the computer-frame velocity error model (Waldmann, 2004). The latter describes the error dynamics with a structure $\Delta\dot{x}'_{NED} = A'(t)\Delta x'_{NED} + B(t)\Delta u$ that fits in with the Kalman filter framework. IMU sensor errors are additive accelerometer bias ∇_b, rate-gyro drift ε_b, and white noise n:

$$\Delta x'_{NED} = \begin{bmatrix} \Delta R_{NED}{}^{T} & \Delta V_{e,NED}{}^{T} & \psi_{NED}{}^{T} \end{bmatrix}^{T} \quad \Delta R_{NED} = \begin{bmatrix} \Delta R_N & \Delta R_E & \Delta R_D \end{bmatrix}^{T} \quad \Delta V_{e,NED} = \begin{bmatrix} \Delta V_N & \Delta V_E & \Delta V_D \end{bmatrix}^{T} \quad \psi_{NED} = \begin{bmatrix} \psi_N & \psi_E & \psi_D \end{bmatrix}^{T}$$

$$\Delta u = \begin{bmatrix} \nabla_b{}^{T} & \varepsilon_b{}^{T} \end{bmatrix}^{T} \quad \nabla_b = \begin{bmatrix} \nabla_{Xb} & \nabla_{Yb} & \nabla_{Zb} \end{bmatrix}^{T} \quad \varepsilon_b = \begin{bmatrix} \varepsilon_{Xb} & \varepsilon_{Yb} & \varepsilon_{Zb} \end{bmatrix}^{T}$$

$$A' = \begin{bmatrix} A_{11} & I_3 & 0_3 \\ A_{21} & A_{22} & A_{23} \\ 0_3 & 0_3 & A_{33} \end{bmatrix} \quad A_{11} = \begin{bmatrix} 0 & \rho_D & -\rho_E \\ -\rho_D & 0 & \rho_N \\ \rho_E & -\rho_N & 0 \end{bmatrix} \quad A_{21} = \text{diag}(-g_0/R_0, -g_0/R_0, 2g_0/R_0)$$

$$A_{22} = \begin{bmatrix} 0 & \rho_D + 2\Omega_D & -\rho_E \\ -(\rho_D + 2\Omega_D) & 0 & \rho_N + 2\Omega_N \\ \rho_E & -(\rho_N + 2\Omega_N) & 0 \end{bmatrix} \quad A_{23} = \begin{bmatrix} 0 & -A_{sp,D} & A_{sp,E} \\ A_{sp,D} & 0 & -A_{sp,N} \\ -A_{sp,E} & A_{sp,N} & 0 \end{bmatrix}_{measured}$$

$$A_{33} = \begin{bmatrix} 0 & \rho_D + \Omega_D & -\rho_E \\ -(\rho_D + \Omega_D) & 0 & \rho_N + \Omega_N \\ \rho_E & -(\rho_N + \Omega_N) & 0 \end{bmatrix} \quad B = \begin{bmatrix} 0_{3x3} & 0_{3x3} \\ D_p^b & 0_{3x3} \\ 0_{3x3} & -D_p^b \end{bmatrix} \quad (10)$$

To estimate the errors in IMU sensors, assuming full observability, the above error vector was augmented with a random constant model of ∇_b and ε_b. Noting Eq. (10), the augmented dynamics is:

$$\Delta\dot{x} = A(t)\Delta x + n \qquad \Delta x \in R^{15} \qquad \Delta x = \begin{bmatrix} \Delta x'_{NED} \\ \Delta u \end{bmatrix} \qquad A = \begin{bmatrix} A' & B \\ 0_{6x9} & 0_6 \end{bmatrix} \qquad (11)$$

3. INDIRECT FEEDFORWARD AND FEEDBACK INS AIDING

The continuous lines in Fig. 2 depict a feedfoward, indirect Kalman filter-based fusion of INS estimates with aiding position and terrestrial velocity, which are output by the processing of observables within the aiding sensors. The term "indirect" refers to error state estimation rather than estimation of the full state. The dashed lines indicate the feedback configuration, in which the INS is reset during operation by subtracting the estimates of misalignment and IMU errors. Noting that subscript a indicates aiding sensor, and measurement y is the difference between the INS solution and the aiding position and velocity, then:

$$R_{INS} = R + \Delta R, \ V_{e,INS} = V_e + \Delta V_e$$

$$y = \begin{bmatrix} \mathbf{R_{INS}} - \mathbf{R_a} \\ \mathbf{V_{e,INS}} - \mathbf{V_{e,a}} \end{bmatrix} = \begin{bmatrix} \Delta\mathbf{R} - \mu \\ \Delta\mathbf{V_e} - \eta \end{bmatrix} \tag{12}$$

Representation of the above aiding differences in the NED coordinate frame yields:

$$\Delta R_N = (\lambda_{INS} - \lambda_a)(R_N + h_a) \qquad \Delta R_E = (\Lambda_{INS} - \Lambda_a)(R_E + h_a)\cos(\lambda_a) \qquad \Delta R_D = -(h_{INS} - h_a)$$

$$\Delta\mathbf{V_{e,NED}} = (\mathbf{V_{e,INS}} - \mathbf{V_{e,a}})_{NED} = \begin{bmatrix} \Delta V_N & \Delta V_E & \Delta V_D \end{bmatrix}^T \tag{13}$$

Ideally, μ and η are white and uncorrelated noise processes in the aiding sensors. However, the processing of observables gives rise to correlation in time and among components of aiding position and velocity. Such correlations are not considered here in the statistical model of measurement errors. Thus, the discrete-time measurement equation in the aided-INS Kalman filter is $y_j=[\Delta R_{NED(j)}^T \; \Delta V_{e,NED(j)}^T]^T = H\Delta x_j + v_j$, where v_j is a zero-mean, white sequence with diagonal covariance $\overline{R}$, and $H=diag(I_6, O_{6x9})$.
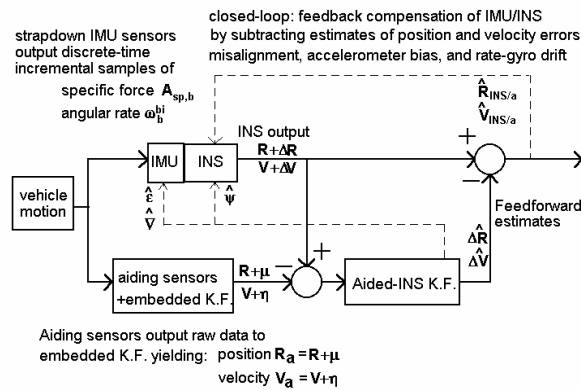

Figure 2 - Indirect feedforward INS-aiding architecture. $\mathbf{V}$ is herein used to denote the terrestrial velocity $\mathbf{V_e}$.

The transformed measurements $A_{sp,NED,m}$, and INS solution-dependent parameters $V_{e,INS}$, R_{INS} and $\mathbf{D_{p,INS}^b}$ in Eq. (11) have been updated at rate $1/T_{nav}=100Hz$. $A(t)$ has been discretized to produce the state transition matrix, that is $\mathbf{\Phi}_k = I + A(kT_{nav})T_{nav}(I + A(kT_{nav})T_{nav}/2)$. Uncertainty in $\mathbf{\Phi}_k$ has been translated into an additive, zero-mean, white noise sequence w_k with diagonal covariance matrix Q, which is related to the linearization error about the diverging INS solution. Q demanded tuning. Filter estimates and respective covariance matrix have been propagated forward in time also with frequency $1/T_{nav}$. Their updates at rate $1/T_a = 1Hz$ occurred when aiding measurements became available. The caret superscript indicates the filter estimate of the error state Δx, and P is the filter-computed covariance of the estimation error. The implemented Kalman filter equations and corresponding computation rates are:

Initialization:

$$\hat{\Delta x}_0^+ = \hat{\Delta x}_0 \;\; ; \; \mathbf{P}_0^+ = \mathbf{P}_0 \;\; ; \; k=0 ; j=1 \tag{14}$$

Propagation until update available – $1/T_{nav}=100Hz$:

$$k = k+1; \; \hat{\Delta x}_k^- = \mathbf{\Phi}_{k-1} \hat{\Delta x}_{k-1}^-$$
$$\mathbf{P}_k^- = \mathbf{\Phi}_{k-1}\mathbf{P}_{k-1}^-\mathbf{\Phi}_{k-1}^T + \mathbf{Q} \tag{15}$$

Update available – $1/T_a=1Hz$:

$$\hat{\Delta x}_j^- = \hat{\Delta x}_k^- \;\; ; \; \mathbf{P}_j^- = \mathbf{P}_k^-$$
$$\mathbf{K}_j = \mathbf{P}_j^-\mathbf{H}^T[\mathbf{H}\mathbf{P}_j^-\mathbf{H}^T + \overline{\mathbf{R}}]^{-1}$$
$$\hat{\Delta x}_j^+ = \hat{\Delta x}_j^- + \mathbf{K}_j[y_j - \mathbf{H}\hat{\Delta x}_j^-]; k=0; \hat{\Delta x}_k^- = \hat{\Delta x}_j^+$$
$$\mathbf{P}_j^+ = [\mathbf{I_{15}} - \mathbf{K}_j\mathbf{H}]\mathbf{P}_j^- \;\; ; \; \mathbf{P}_k^- = \mathbf{P}_j^+ \;\; ; \; j=j+1 \tag{16}$$

Return to propagation stage.

$$\overline{\mathbf{R}} = diag((3[m])^2\mathbf{I_3}, (0.05[m/s])^2\mathbf{I_3}) \qquad\qquad \mathbf{Q} = T_{nav}.diag((1[m])^2\mathbf{I_3}, (10^{-5}[m/s])^2\mathbf{I_3}, \mathbf{0_{1x9}})$$

$$\mathbf{P_0} = \mathrm{diag}((10[\mathrm{m}])^2\mathbf{I_3}, (0.5[\mathrm{m/s}])^2\mathbf{I_3}, \mathbf{Z}, (3\mathbf{I_3}\nabla_\mathrm{b}[\mathrm{m/s^2}])^2, (3\mathbf{I_3}\varepsilon_\mathrm{b}[\mathrm{rd/s}])^2)$$

$$\mathbf{Z} = \mathrm{diag}((\nabla_\mathrm{E}/\mathrm{g}[\mathrm{rd}])^2, (\nabla_\mathrm{N}/\mathrm{g}[\mathrm{rd}])^2, ((-\varepsilon_\mathrm{E} + \Omega_{\mathrm{D}0}\nabla_\mathrm{E}/\mathrm{g})/\Omega_{\mathrm{N}0}[\mathrm{rd}])^2)$$

$$\begin{bmatrix} \nabla_\mathbf{NED}^{\mathrm{T}} & \varepsilon_\mathbf{NED}^{\mathrm{T}} \end{bmatrix}^{\mathrm{T}} = \mathrm{diag}(\mathbf{D}_{\mathbf{p,INS}}^\mathbf{b}, \mathbf{D}_{\mathbf{p,INS}}^\mathbf{b}) \begin{bmatrix} \nabla_\mathbf{b}^{\mathrm{T}} & \varepsilon_\mathbf{b}^{\mathrm{T}} \end{bmatrix}^{\mathrm{T}}$$

P_0 reflected the initial uncertainty in the estimation error. The diagonal form of Z represents the impact of IMU errors ∇_{NED} and ε_{NED} on the uncertainty about initial misalignment angle $\psi_{NED}(0)$. Due to model mismatch, the residual sequence $r_j = y_j - H\,\hat{\Delta x}_j^-$ at instants multiple of T_a has been monitored to ensure statistical consistency (Bar-Shalom and Li, 1993). Adequate tuning of Q should produce a zero-mean, white, Gaussian residual sequence with covariance matrix $S_j = HP_j^- H^T + \overline{R}$. Had a position or velocity residual component been found outside ±3 times the square root of the corresponding element in the diagonal of S, the corresponding position or velocity error variance in P was reset to $(3m)^2$ and $(0.3m/s)^2$, respectively. The corresponding off-diagonal elements in P were also altered to keep the cross-correlation coefficients unchanged by the reset.

3.1. Maneuvers for observability enhancement

Goshen-Meskin and Bar-Itzhack (1990) modeled maneuvers during the IFA phase of a GINS with 20 seconds, piece-wise constant (PWC), 0.1g specific force segments. Consequently, $\mathbf{D}_\mathbf{p}^\mathbf{b} = \mathbf{I}$, and $\mathbf{A_{23}}$ in (11) was the single PWC, significantly time-varying block in $\mathbf{A}(t)$. IMU rotation, however, violates conditions for valid SOM analysis because $\mathbf{D}_\mathbf{p}^\mathbf{b}$ in $\mathbf{B}(t)$ varies continuously. The impact of PWC acceleration segments and IMU rotation on estimation accuracy, *both at a known location on the ground and during IFA*, is gauged with the filter-computed standard deviation of the estimation error and, as in Pittelkau (2005), one realization. Aiding position and velocity measurements, respectively $\mathbf{R_a}$ and $\mathbf{V_{e,a}}$, have been generated from ground-truth corrupted by additive Gaussian, zero-mean, white noise with covariance matrix $\overline{\mathbf{R}}$. IMU rotation with respect to the vehicle has been simulated with IMU attitude ground-truth in terms of yaw, pitch, and roll relative to the NED coordinate frame (Bar-Itzhack, 1977):

$$\psi = \mathrm{s}(2\pi t/300) + 0.5\,\mathrm{s}(2\pi t/1.7)[\mathrm{rd}]$$
$$\theta = \mathrm{s}(2\pi t/300) + 0.5\,\mathrm{s}(2\pi t/1.7 + 0.3)[\mathrm{rd}]$$
$$\phi = \mathrm{s}(2\pi t/300) + 0.5\,\mathrm{s}(2\pi t/0.85)[\mathrm{rd}] \quad t \in [0,200][\mathrm{s}] \tag{17}$$

The GINS stand-alone solution was simulated by enforcing that $\psi \equiv \theta \equiv \phi \equiv 0$, generating IMU data, and solving Eq. (6) and Eq. (7). In this case, $X_b \equiv N$, $Y_b \equiv E$, and $Z_b \equiv D$. Each rate-gyro has been corrupted by drift $\varepsilon_{Xb} = \varepsilon_{Yb} = \varepsilon_{Zb} = 2\,°/h$ and additive zero-mean, white noise with standard deviation $\sigma_\varepsilon = 1\,°/h$, and integrated between consecutive sensor samples to yield the incremental angular measurements. Given the initial position and terrestrial velocity, and ground acceleration $\dot{V}_N, \dot{V}_E, \dot{V}_D$ which the IMU was subject to, the NED ground-truth specific force $A_{sp,NED,t}$ was obtained from Eq. (6). From IMU attitude ground-truth in Eq. (17), $D_b^t A_{sp,NED,t}$ has been computed, and each accelerometer corrupted by bias $\nabla_{Xb} = \nabla_{Yb} = \nabla_{Zb} = 3mg$ and additive zero-mean, white noise with standard deviation $\sigma_\nabla = 1mg$. Integration between consecutive sensor samples resulted in the incremental thrust velocity measurements. As an example, the true position error of the stand-alone INS for a stationary GINS at a known location is seen in Figure 3. Error divergence is the main motivation for fusion of low-cost INS and aiding sensors.
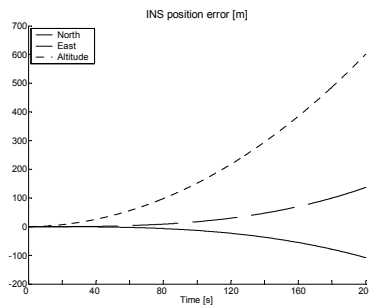

Figure 3 – Stationary GINS true position error (m). North (dash), East (continuous), and altitude (dot).

Motion 1 aimed to show whether a constant, long-duration acceleration can enhance observability, though its ultimate velocity is surely not attainable by a low-cost host vehicle. With $\lambda(0)=23°12'S$, $\Lambda(0)=45°52'W$, and $h(0)=600m$ as the initial location at ITA facilities, Motion 1 consisted of constant ground acceleration $a=5m/s^2$ (Bar-Itzhack, 1977):

$$V_N = V_E = -V_D = 300 + at\,[m/s] \qquad t \in [0,200]\,[s] \tag{18}$$

With the same initial location and terrestrial velocity, Motion 2 comprised five PWC, 40s ground acceleration segments as shown in Tab. 1.

4. FEEDFORWARD ESTIMATION, SWITCH TO FEEDBACK, AND INS CALIBRATION: RESULTS

Making use of solely the indirect feedforward fusion seen in Fig. 2, Tab. 2 summarizes the effect of the maneuvers on one realization of the estimation error of IMU sensor errors and misalignment at $t=200s$, and respective filter-computed standard deviation. The results show that the combination of concatenated acceleration maneuvers in distinct directions and rotating the IMU provide the most accurate estimates. The simulations showed that error propagation of a GINS at rest and in cruise are seen to be similar because of negligible horizontal specific forces in both conditions. Thus, Tab.2 display only the case of the stationary GINS.

Table 1 - Motion 2 ground acceleration segments

Segment	$\dot{V}_N$	$\dot{V}_E$	$\dot{V}_D$
1	0	0	0
2	a	0	0
3	0	a	0
4	a	a	0
5	0	0	-a

Table 2 – Effect of maneuvers on accelerometer bias, rate-gyro drift, and INS misalignment estimation error after *200s*
Indirect feedforward of error estimates only.

Maneuver	∇_{Xb} mg	∇_{Yb} mg	∇_{Zb} mg	ε_{Xb} deg/h	ε_{Yb} deg/h	ε_{Zb} deg/h	ϕ_N arcsec	ϕ_E arcsec	ϕ_D arcsec
Stationary GINS (IMU)									
Est. Error	–2.5972	–0.6968	–0.0069	0.0352	–0.2800	–5.0900	-143	590	–4.45E3
Std. Dev.	2.8401	2.8400	0.0136	0.2784	2.1150	5.8900	589	534	2.76E4
Accelerated GINS									
Motion 1 Est. Error	1.6918	–3.4092	–0.6778	0.1579	–0.2059	–0.5456	123	425	–1890
Std. Dev.	5.6623	3.0535	0.9536	0.9101	0.7899	3.2297	256	468	1276
Motion 2 Est. Error	0.2395	–0.0265	0.0659	–0.0514	–0.1418	0.3506	–7.77	–56.0	–48.1
Std. Dev.	0.1031	0.0704	0.0266	0.0916	0.0818	0.3727	12.9	18.8	38.0
Rotating IMU, stationary host									
Est. Error	–0.0849	–0.1080	–0.0278	–0.5973	–1.3490	–0.5518	–12.4	–10.7	–1.10E4
Std. Dev.	0.0679	0.1010	0.0222	0.9960	2.6080	0.9822	15.7	19.9	1.86E4
Rotating IMU and Motion 2									
Est. Error	–0.0341	–0.0485	–0.0555	0.0321	0.0100	0.0016	–24.5	–3.92	–9.82
Std. Dev.	0.0361	0.0727	0.0486	0.2070	0.0830	0.1586	10.7	11.1	17.2

Figure 4 shows the ± 1–sigma filter–computed standard deviation of the estimation error (i.e. filter uncertainty) and one realization of IMU sensor error estimation for Motion 2 combined with IMU rotation. Figure 5 shows the corresponding misalignment. The figures clearly indicate the significant estimation error in the initial acceleration segments, which precluded the use of indirect feedback fusion and INS calibration with estimates of IMU errors and misalignment right from the start. Such attempts failed because of filter divergence. The same was observed both for GINS and rotating IMU mechanizations. Thus, switching from feedforward to feedback of error estimates and the corresponding IMU calibration occured at $t=195s$. Figure 5 shows how the maneuvers improved the misalignment estimation accuracy, notably in azimuth, which is weakly observable when the IMU is stationary on the ground. After the switch to feedback of error estimates, the INS solution to the attitude DCM computed with Eq. (7) was corrected with the estimated misalignment as follows. Recalling Eq. (9) and Fig. 2:

$$\hat{\phi} = \hat{\psi} + \delta\hat{\theta} \tag{19}$$

$$\hat{\mathbf{D}}_{\mathbf{p}}^{\mathbf{t}} = \begin{bmatrix} 1 & \hat{\phi}_D & -\hat{\phi}_E \\ -\hat{\phi}_D & 1 & \hat{\phi}_N \\ \hat{\phi}_E & -\hat{\phi}_N & 1 \end{bmatrix} \text{ and } \hat{\mathbf{D}}_{\mathbf{t}}^{\mathbf{b}} = \hat{\mathbf{D}}_{\mathbf{t}}^{\mathbf{p}} \mathbf{D}_{\mathbf{p},INS}^{\mathbf{b}} = (\hat{\mathbf{D}}_{\mathbf{p}}^{\mathbf{t}})^{\mathrm{T}} \mathbf{D}_{\mathbf{p},INS}^{\mathbf{b}}$$

(20)
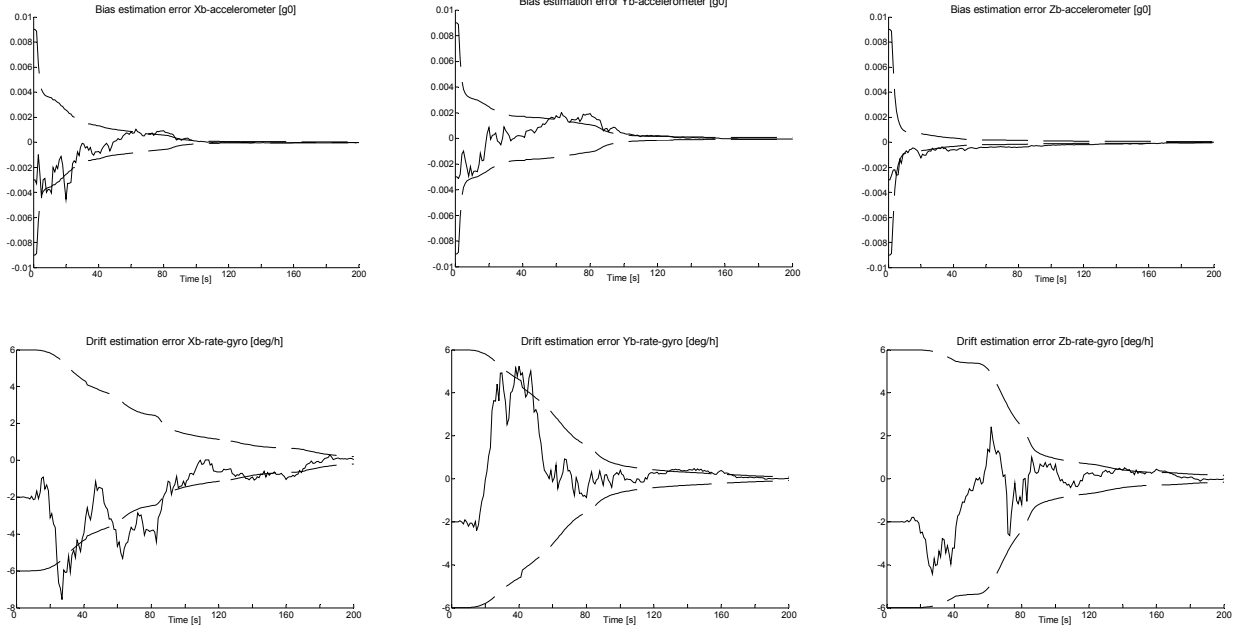
Figure 4 – Bias (g_0) and drift (deg/h) estimation error − motion 2 and rotating IMU, indirect feedforward fusion.
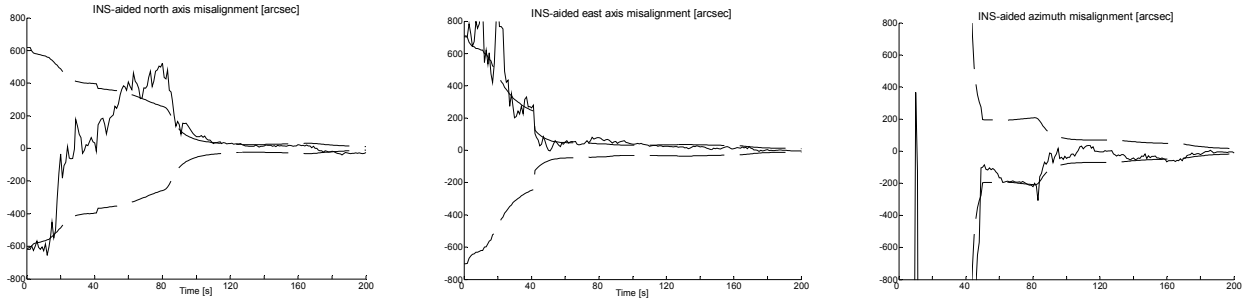

Figure 5 - Misalignment estimation error (arcsec) - motion 2 and rotating IMU, indirect feedforward fusion.

Throughout the simulation, both before and after switching from feedforward to the feedback configuration the accuracy of the estimated DCM was evaluated by two performance measures. A convergence index *J* indicated how close the estimated DCM was from the ground-truth, whereas an orthogonality index *F* measured the degree of orthonormality of the rows (columns) of the estimated DCM:

$$J = \mathrm{trace}\left[\left(\hat{\mathbf{D}}_{\mathbf{t}}^{\mathbf{b}} - \mathbf{D}_{\mathbf{t}}^{\mathbf{b}} \right)^{\mathrm{T}} \left(\hat{\mathbf{D}}_{\mathbf{t}}^{\mathbf{b}} - \mathbf{D}_{\mathbf{t}}^{\mathbf{b}} \right) \right] \geq 0$$

(21)

$$F = \mathrm{trace}\left[\left(\hat{\mathbf{D}}_{\mathbf{t}}^{\mathbf{b}} \mathbf{D}_{\mathbf{b}}^{\mathbf{t}} - \mathbf{I} \right)^{\mathrm{T}} \left(\hat{\mathbf{D}}_{\mathbf{t}}^{\mathbf{b}} \mathbf{D}_{\mathbf{b}}^{\mathbf{t}} - \mathbf{I} \right) \right] \geq 0$$

(22)

Figure 6 and Fig. 7 depict the statistics of a Monte Carlo simulation with 20 realizations concerning the position estimation error, and velocity estimation error, respectively. The results are indeed encouraging regarding the concept of IFA with a rotating IMU relative to the vehicle. Figure 8 shows a typical realization of both position and velocity errors at the INS output seen in Fig.2. Previous results showed that feedforward of the error estimates compensate for most of the errors, and the compensated INS signals are then sent to other subsystems on-board the host vehicle. However, linearization errors in the filter model about the diverging INS output continue to increase. Filter divergence is then avoided by switching to the feedback configuration. Then, IMU calibration by means of removal of estimated biases and drifts, and INS output correction with the estimated misalignment, velocity, and position errors result in a drastic reduction of INS output error. In this condition, the filter model is linearized about a far less incorrect trajectory.
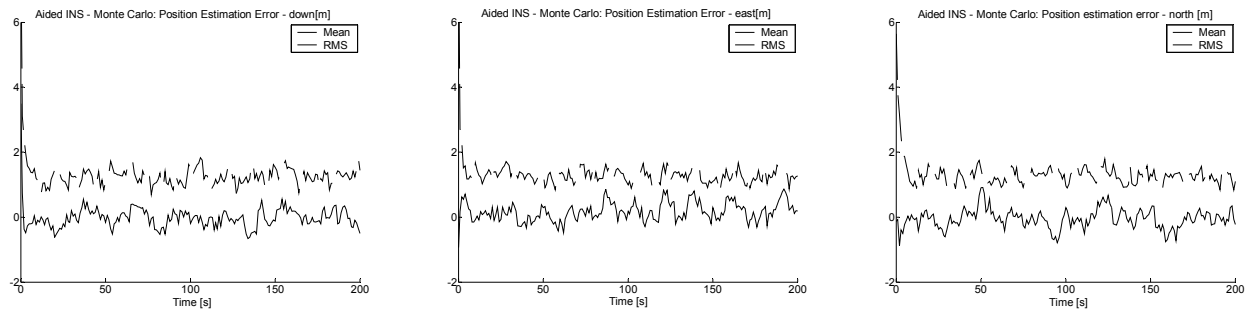
Figure 6 – Monte Carlo simulation. Position estimation error (m) - motion 2 and rotating IMU.
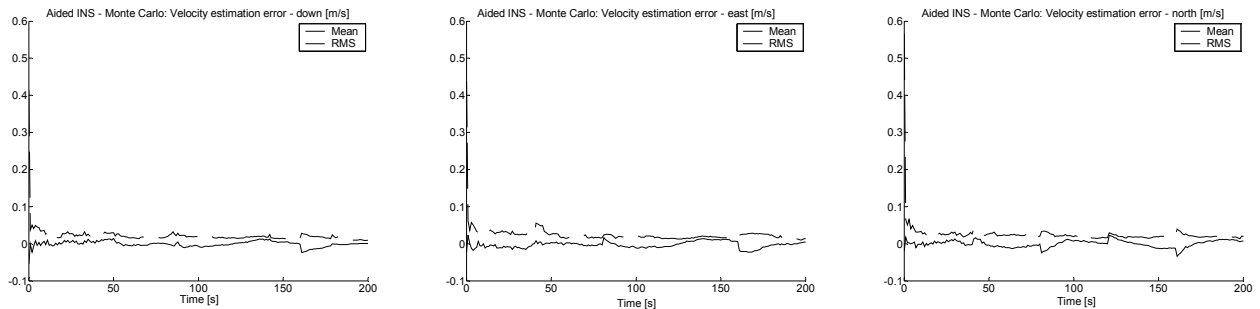

Figure 7 – Monte Carlo simulation. Velocity estimation error (m/s) - motion 2 and rotating IMU.
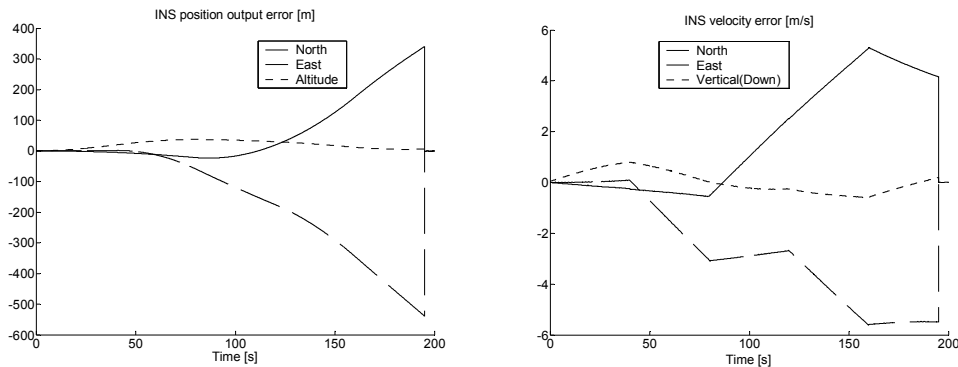

Figure 8 – One realization of INS position and velocity output error - motion 2 and rotating IMU – switch at t=195s.

Figure 9 shows the performance indices regarding the computation of the DCM. The results depict a typical realization, and the Monte Carlo simulation with 20 realizations, the mean, the minimum, and the maximum index value. Notice the positive effect of the initial maneuvers on DCM estimation accuracy.
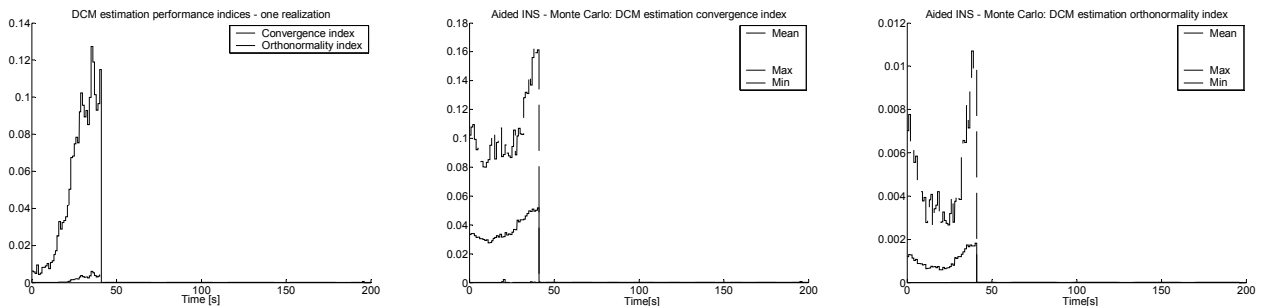

Figure 9 – DCM estimation performance indices - motion 2 and rotating IMU – switch at t=195s.

5. CONCLUSION

The results showed the benefit of continuously rotating the IMU during the stationary initial alignment on the ground at a known location for faster, more accurate estimation of accelerometer bias. Previous work by Lee *et al.* (1993) investigated PWC, multiposition initial alignment rather than continuously changing IMU attitude. IMU rotation does not demand the fine engineering, delicate assembly, and accurate moving parts found in a GINS.

Lack of observability caused by insufficient IMU maneuvering produced optimistic filter performance and biased estimation. Such detrimental qualities were significantly mitigated by means of combining IMU rotation with PWC acceleration segments. Thus, improved estimates of accelerometer bias, misalignment, especially in azimuth, and rate-gyro drift become available after maneuvers. Then, a switch from feedforward configuration to a feedback one took place, and the error estimates employed for on-the-fly IMU calibration and removal of misalignment.

The diverging stand-alone INS solution causes model mismatch in the Kalman filter, which was neglected in a previous covariance analysis of PWC dynamics during the IFA phase by Goshen-Meskin and Bar-Itzhack (1990). The indirect feedforward approach with the linearized Kalman filter is only appropriate for short-term applications because model mismatch may cause filter divergence. For long duration applications, the extended Kalman filter arises by means of INS reset. In such a case, the results show that caution should be exercised when designing the feedback logic for INS reset. Full removal of misalignment, accelerometer bias, and rate–gyro drift estimates should occur *after* the diagonal values of filter covariance **P** decay to safe values determined by simulation to avoid filter divergence.

6. ACKNOWLEDGEMENTS

7. REFERENCES

Adam, A., Rivlin, E., and Rotstein, H. (1999). Fusion of Fixation and Odometry for Vehicle Navigation. *IEEE Transactions on Systems, Man, and Cybernetics – Part A: Systems and Humans*, 29(6):593-603.

Bar-Itzhack, I.Y. (1977). Navigation Computation in Terrestrial Strapdown Inertial Navigation System. *IEEE Transactions on Aerospace and Electronic Systems*, 13(6):679-689.

Bar-Itzhack, I.Y. (1978). Corrections to Navigation Computation in Terrestrial Strapdown Inertial Navigation System. *IEEE Transactions on Aerospace and Electronic Systems*, 14(3):542-544.

Bar-Itzhack, I.Y., and Berman, N. (1988). Control Theoretic Approach to Inertial Navigation Systems. *Journal of Guidance, Control, and Dynamics*, 11(3):237-245.

Bar-Shalom, Y. and Li, X.-R. (1993). Estimation and Tracking: Principles, Techniques, and Software, Artech House, Boston, USA.

Eck, C. and Geering, H.P. (2000). Error Dynamics of Model Based INS/GPS Navigation for an Autonomously Flying Helicopter. *AIAA Guidance, Navigation, and Control Conference*, Denver, CO, USA, 1-9.

Goshen-Meskin, D., and Bar-Itzhack, I.Y. (1990). Observability Analysis of Piece-Wise Constant Systems with Applications to Inertial Navigation. *Proceedings of the 29th Conference on Decision and Control*, Honolulu, Hawaii, 821-826.

Hafskjold, B. H., Jalving, B., Hagen, P.E., and Gade,K. (2000). Integrated Camera-Based Navigation. *Journal of Navigation*, 52(2):237-243.

Jekeli, C. (1997). Gravity on Precise, Short-Term, 3-D Free-Inertial Navigation, *Navigation: Journal of The Institute of Navigation*, 44(3):347-357.

Lee, J.G., Park, C.G., and Park, H.W. (1993). Multiposition Alignment of Strapdown Inertial Navigation System, *IEEE Transactions on Aerospace and Electronic Systems*, 29(4):1323-1328.

Pittelkau, M.E. (2005). Calibration and Attitude Determination with Redundant Inertial Measurement Units, *Journal of Guidance, Control, and Dynamics*, 28(4):743-752.

Roumeliotis, S.I., Johnson, A.E., and Montgomery, J.F. (2002). Augmenting Inertial Navigation with Image-Based Motion Estimation. *Proceedings of the IEEE International Conference on Robotics and Automation*, Washington, DC, USA, 4326-4333.

Savage, P.G. (1998). Strapdown Inertial Navigation Integration Algorithm Design Part 2: Velocity and Position Algorithms. *Journal of Guidance, Control, and Dynamics*, 21(2):208-211.

Siouris, G. M. (1993). Aerospace Avionics Systems: A Modern Synthesis, Academic Press, San Diego, USA.

Wagner, J.F., and Wienecke T. (2003). Satellite and Inertial Navigation − Conventional and New Fusion Approaches, Control Engineering Practice, 11:543-550.

Waldmann, J. (2003). Sculling and Scrolling Effects on the Performance of Multirate Terrestrial Strapdown Navigation Algorithms. *Proceedings of the 17th International Congress of Mechanical Engineering COBEM2003*, São Paulo, SP, Brazil, ISBN 85-85769-14-9.

Waldmann, J. (2004). A Derivation of the Computer-Frame Velocity Error Model for INS Aiding. *Proceedings of the 15th Brazilian Automation Conference (Congresso Brasileiro de Automática)*, Gramado, RS, Brazil, ISBN 85-85769-14-9.

8. RESPONSIBILITY NOTICE

The author is the only responsible for the printed material included in this paper.